

# F2F-AP: Flow-to-Future Asynchronous Policy for Real-time Dynamic Manipulation

Haoyu Wei Xiuwei Xu<sup>†</sup> Ziyang Cheng Hang Yin Angyuan Ma  
 Bingyao Yu Jie Zhou Jiwen Lu  
 Department of Automation, Tsinghua University  
<https://why-peace.github.io/F2F-AP/>

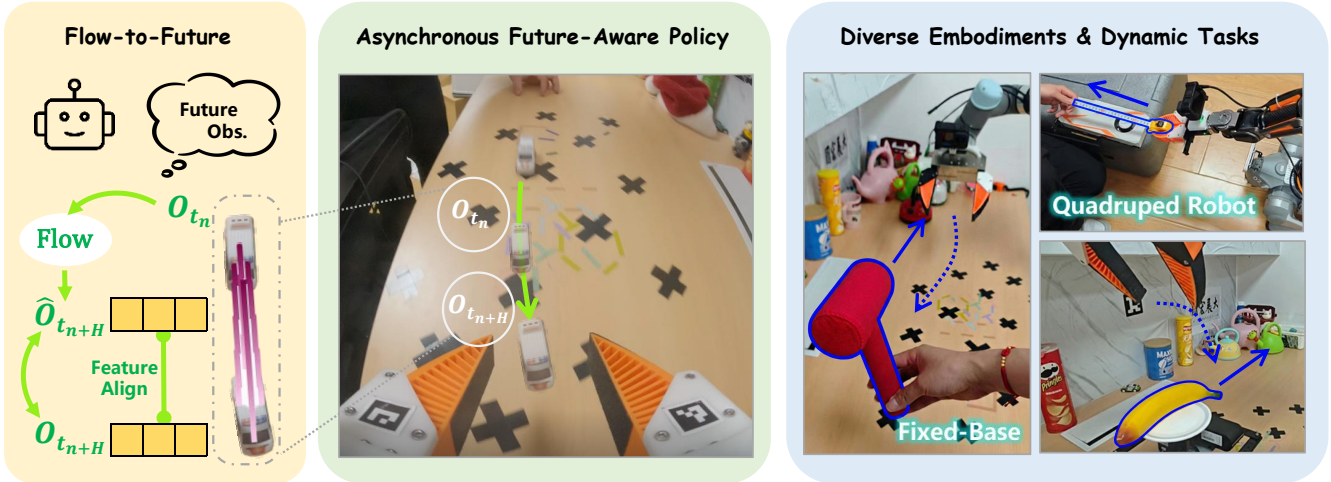


Fig. 1: **Flow-to-Future Asynchronous Policy (F2F-AP)**. F2F-AP is an asynchronous robot manipulation policy that explicitly incorporates future observations. By predicting future observations in the form of optical flow, it enhances the model’s understanding of the motion trends of interacting objects. F2F-AP is transferable to diverse embodiments and yields significant performance improvements in dynamic tasks.

**Abstract**—Asynchronous inference has emerged as a prevalent paradigm in robotic manipulation, achieving significant progress in ensuring trajectory smoothness and efficiency. However, a systemic challenge remains unresolved, as inherent latency causes generated actions to inevitably lag behind the real-time environment. This issue is particularly exacerbated in dynamic scenarios, where such temporal misalignment severely compromises the policy’s ability to interpret and react to rapidly evolving surroundings. In this paper, we propose a novel framework that leverages predicted object flow to synthesize future observations, incorporating a flow-based contrastive learning objective to align the visual feature representations of predicted observations with ground-truth future states. Empowered by this anticipated visual context, our asynchronous policy gains the capacity for proactive planning and motion, enabling it to explicitly compensate for latency and robustly execute manipulation tasks involving actively moving objects. Experimental results demonstrate that our approach significantly enhances responsiveness and success rates in complex dynamic manipulation tasks.

## I. INTRODUCTION

Despite recent impressive advancements in robotic manipulation [18, 42, 43], the inherent computational latency of policy inference often hinders real-world deployment. Under straightforward synchronous execution strategies, robots frequently

exhibit sluggish and discontinuous motion, severely compromising the system’s responsiveness. Consequently, there is a growing trend towards adopting asynchronous inference frameworks, which parallelize model inference with action execution to significantly improve response speeds.

In asynchronous inference, action chunking serves as the foundation for these methods. Under this paradigm, the model predicts a sequence of actions covering multiple future timesteps, allowing the robot to infer the next action chunk during the execution of the corresponding actions in the current chunk. However, this introduces two critical issues. First, since chunked actions are aligned to the start of inference, inference latency renders the initial actions outdated upon execution, forcing them to be discarded. Second, compounding latencies cause the policy to persistently lag behind the evolving environment and robot state. This problem is particularly acute in dynamic tasks. While static tasks might rely on a single optimal trajectory, dynamic scenarios involve highly complex and continuously shifting action spaces.

A representative recent work, VLASH [35], mitigates the issue by conditioning policies on anticipated future proprioceptive states. By directly predicting actions for the exact moment of execution, VLASH eliminates the need to discard the initial steps of the action chunk, thereby achieving

<sup>†</sup> Project Leader

smoother connections between successive trajectories to a certain extent. However, a critical flaw still remains: the temporal misalignment between stale visual observations and anticipated future states. Without access to future visual cues, the policy is forced to “guess” future actions based on insufficient, outdated visual information rather than accurately “inferring” them from a synchronized real-time context. Consequently, achieving robust and accurate real-time dynamic manipulation in asynchronous policy remains an open challenge.

To address these challenges, we propose **Flow-to-Future Asynchronous Policy (F2F-AP)**, a future-aware framework tailored for real-time dynamic robotic manipulation, as shown in Fig. 1. F2F-AP utilizes the predicted object flow of interacting objects as a dynamic scene representation to synthesize future visual observations. Furthermore, we propose a *flow contrastive learning* objective to bridge the gap between predicted and ground-truth future observations, minimizing feature discrepancy to guarantee the fidelity of the anticipated context. By explicitly modeling system latency within an asynchronous pipeline, F2F-AP successfully generates action chunks that perfectly align with real-world timing, ensuring naturally connected trajectories. Simultaneously, the synthesized future observations effectively compensate for the information deficit caused by latency in dynamic tasks. Extensive experiments demonstrate that F2F-AP achieves significantly superior performance over prior methods across multiple dynamic tasks on two distinct hardware platforms, fully validating the necessity and effectiveness of our proposed design.

In summary, the main contributions of F2F-AP are:

- **F2F Module.** We propose the F2F module to predict object flow as a representation of motion trends in dynamic scenes. These predictions are encoded as future-aware observations to enhance the policy’s input context.
- **Flow Contrastive Learning.** We introduce a flow contrastive learning objective to align the features of flow-based predictions with ground-truth future observations, minimizing the feature discrepancy between them.
- **Real-World System.** We deploy F2F-AP on both a fixed-base robotic arm and a quadruped mobile manipulator, validating the superior capability of this future-aware asynchronous policy in highly dynamic tasks.

## II. RELATED WORK

### A. Affordance-based Manipulation

In robotic manipulation tasks, the gap between raw linguistic or visual inputs and the corresponding action outputs makes it challenging for policies to implicitly learn intermediate knowledge such as object localization and functionality. To bridge this gap and enhance scene understanding, various forms of affordances have been integrated into manipulation policies, such as object-centric instance [1, 9, 23, 26, 49], keypoint [12–14, 25, 32], using foundation model [16, 19, 24] and implicit neural fields [7, 31, 41].

The most relevant approaches to our work are those that utilize flow-based affordances. On one hand, flow or point-

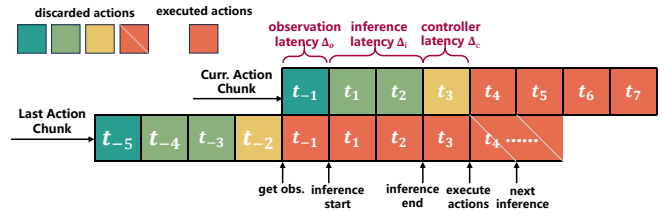


Fig. 2: **Decomposition of system latency.** The total latency ( $\Delta_o + \Delta_i + \Delta_c$ ) results in a temporal misalignment where the initial frames of the predicted trajectory lag behind the real-world state, invalidating them for execution.

trajectory serves as the embodiment-agnostic unified representation [8, 36, 44, 46], facilitating the transfer of manipulation data between different domains, from human demonstrations to robotic manipulation for instance. On the other hand, flow acts as a high-level interface indicating how to act [2, 11, 17, 40, 48, 51], so that the policy can generate actions according to the flow, or directly from motion prediction [33]. While these studies have made substantial contributions to exploiting the utility of flow in manipulation tasks, they primarily focus on how interactive objects should be moved within static environments, while overlooking the spontaneous motion of the objects themselves. In contrast, F2F-AP characterizes motion trends through object flow prediction and encoding future observational features, thereby expanding the role of flow in real-time dynamic scenarios.

### B. Asynchronous Inference

The action chunk [5, 22, 50] is introduced to enable robots to generate actions for multiple future time steps simultaneously, while asynchronous inference [29, 30] is employed to parallelize action chunk inference with action execution to achieve higher deployment frequencies and smoother execution on physical systems. However, asynchronous inference often suffers from trajectory discontinuities. Existing studies [3, 4, 35, 39] have attempted to ensure smooth transitions between consecutive action chunks by incorporating trajectory inpainting, state-conditional inputs, or future states during inference or training. Despite these efforts, such methods fail to address the intrinsic issue that actions lag behind the evolving environment because of latency. To solve this problem, F2F-AP innovatively incorporates a future-observation synthesis module, empowering the policy to plan ahead and compensate for latency. This reduces trajectory redundancy during real-world deployment and further enhances the efficiency of asynchronous inference.

## III. METHOD

This section begins by clarifying the obstacles facing asynchronous robotic policy inference. Next, we elaborate on our core contributions: the Flow2Future Module and Flow Contrastive Learning. The section closes with an overview of the F2F-AP architecture and inference pipeline.

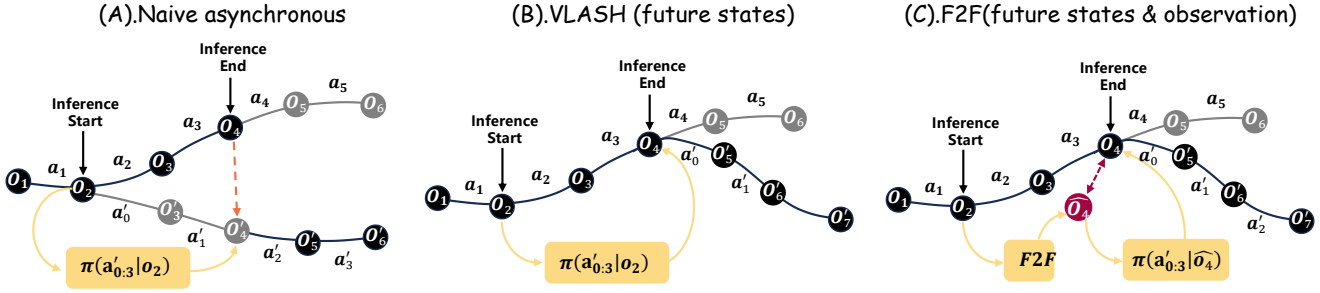


Fig. 3: **Analysis of Asynchronous Inference.** The policy  $\pi(\mathbf{a}|\mathbf{s}, \mathbf{o})$  maps inputs of observations and robot states to action sequences. From left to right, the policy sequentially incorporates future states and predicted observations as augmented context. These additions respectively resolve the trajectory discontinuity caused by state lag and the temporal misalignment of actions resulting from information lag.

#### A. Problem Statement.

Asynchronous inference for dynamic tasks in real world using robotic policy is challenging due to the delayed actions caused by systemic latency. As shown in Fig. 2, the total system latency primarily stems from three components:

- **Observation Latency** ( $\Delta_o$ ): The time delay inherent in sensor acquisition and transmission, meaning the observation used for inference already lags behind the current state.
- **Inference Latency** ( $\Delta_i$ ): The computational time consumed by the model to generate a policy output.
- **Controller Latency** ( $\Delta_c$ ): The delay introduced by the low-level controller during action execution.

In summary, during the total system latency  $\Delta_{\text{total}} = \Delta_o + \Delta_i + \Delta_c$ , a robot operating under an asynchronous inference paradigm continues to execute actions from the current chunk. We define the parameter  $H$  to denote the number of action steps executed during this latency within a single cycle.

**Preliminary.** Asynchronous inference has increasingly become the standard paradigm for deploying robotic policies in real-world settings, as illustrated in Fig. 3. A naive asynchronous policy can be formulated as:

$$\pi(\mathbf{a}_{t:t+n}|\mathbf{s}_t, \mathbf{o}_t) \quad (1)$$

In this paradigm, the robot’s proprioceptive state  $\mathbf{s}_t$  and visual observation  $\mathbf{o}_t$  are strictly temporally aligned, which provides a stable foundation for the model’s predictions. However, due to the inherent system latency during asynchronous execution, the first  $H$  actions in the predicted chunk are already outdated by the time inference completes and must be discarded. Furthermore, because the output actions and the robot’s actual position at the time of execution are mismatched, the resulting trajectory is inherently non-smooth, typically necessitating the use of additional action fusion algorithms to stitch consecutive predictions. Such limitation proves even more detrimental in dynamic tasks.

Alternatively, VLASH [35] proposes a new method from a training perspective, formulating the policy as:

$$\pi(\mathbf{a}_{t+H:t+H+n}|\mathbf{s}_{t+H}, \mathbf{o}_t) \quad (2)$$

By utilizing the anticipated future proprioceptive state  $\mathbf{s}_{t+H}$  as an anchor, VLASH directly outputs actions corresponding to the exact moment of execution. This approach theoretically eliminates the need for complex action fusion and effectively achieves trajectory smoothness. However, VLASH introduces a new critical limitation: the temporal misalignment between the lagging visual context  $\mathbf{o}_t$  and the advanced proprioceptive state  $\mathbf{s}_{t+H}$ . This input imbalance makes it highly difficult for the policy to maintain stable outputs, ultimately failing to correctly and robustly respond to the rapidly evolving environments inherent in dynamic interaction tasks.

**Overview.** F2F-AP aims to resolve the latency problem inherent in asynchronous policies by utilizing temporally aligned future proprioceptive states and visual observations, which can be formulated as follows:

$$\pi(\mathbf{a}_{t+H:t+H+n}|\mathbf{s}_{t+H}, \hat{\mathbf{o}}_{t+H}) \quad (3)$$

First, F2F-AP employs predicted object flow as a bridge to synthesize future observations, ensuring alignment with the ground truth within the feature space. Furthermore, the action chunks generated by F2F-AP are strictly aligned with the exact moment of execution, effectively eliminating the need for discarding initial  $H$  action steps or employing post-hoc action fusion algorithms. Through this design, F2F-AP substantially improves the model’s performance on dynamic tasks.

#### B. Flow2Future Module

In order to predict the future observation, a naive approach to synthesizing future observations would be to directly fine-tune off-the-shelf video generation models [21, 38, 45] on the target tasks. However, current video generation models typically demand seconds of inference time per generation, rendering them entirely incapable of handling dynamic tasks that require rapid responses.

In contrast, we propose the Flow2Future (F2F) module, which leverages predictive object flow as a bridge between current and future observations. The flow predictor employed in F2F module provides an effective and significantly lightweight alternative, making it better suited for real-time deployment on physical robotic systems. The model architecture could be

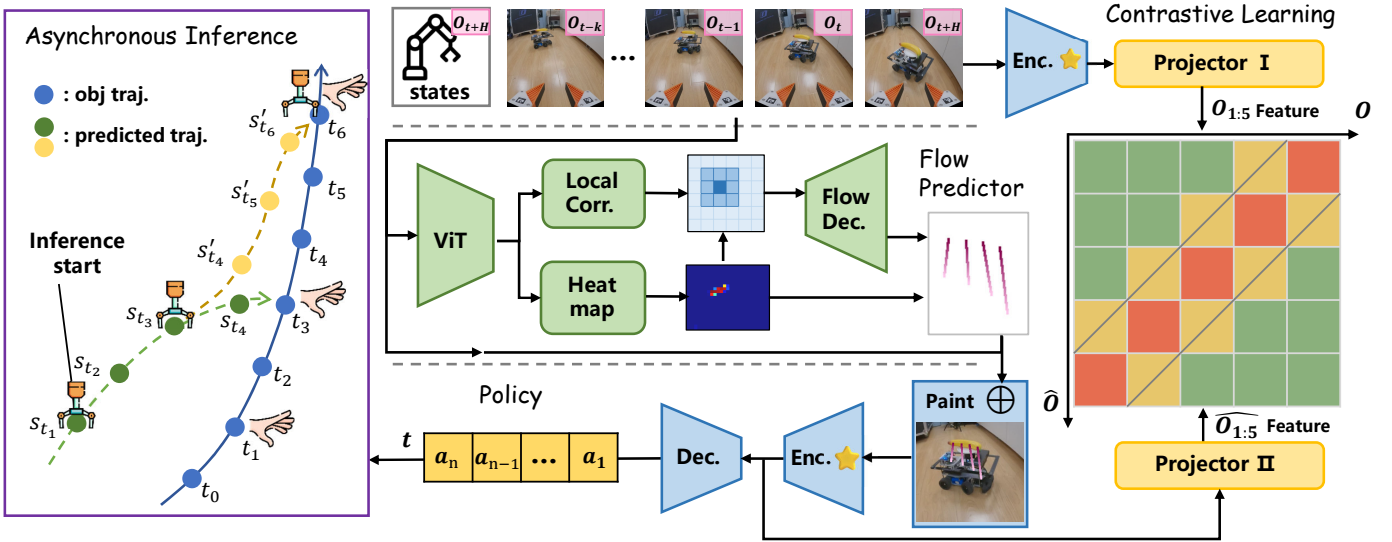


Fig. 4: **Overview of the pipeline.** **Left:** Illustration of the asynchronous inference achieved by F2F-AP. The model plans from a future state  $s_{t_3}$  towards the anticipated position  $t_6$  of the interacting object at timestamp  $t_1$ , enabling advance planning and motion despite real-world system latency. **Middle:** The model takes robot states and multi-frame RGB images as input. A *Flow Predictor* extracts object flow to synthesize augmented future observations, which are then processed by the *Policy* as future observation to generate action chunks. **Right:** We introduce contrastive learning to minimize the feature distance between predicted and real future observations. the ★ indicates that these features share the same encoder.

found in Appendix B.

**Heatmap-Based Flow Predictor.** F2F aims to construct a spatio-temporal visual model that predicts the motion trends of target objects through feature evolution, as shown in the flow predictor part of Fig. 4.

During the training of the sparse object flow predictor, matching the predicted flows with the ground truth for loss computation presents a critical challenge. The ordering of the ground truth elements lacks physical significance, resulting in arbitrary indexing without fixed correspondence across different samples. For instance, a flow point tracking a bottle’s neck might be indexed first in Episode A but last in Episode B. Consequently, applying standard one-to-one or minimum-distance losses—such as enforcing a strict index correspondence or utilizing the Hungarian algorithm—would disrupt the mapping between visual features and spatial coordinates, ultimately forcing the model to converge to an averaged flow as a trivial solution.

To address this, F2F adopts a multi-branch decoder centered on heatmap prediction instead of naive regression. Formally, the object flow prediction  $\mathbf{f}$  is defined as a composition of a refined starting position and a motion displacement vector:

$$\mathbf{f}_{t \rightarrow t+H} = \left[ \underbrace{S(H(Z_v))}_{\text{coarse}} + \underbrace{D_{\text{off}}(Z_v, Z_h)}_{\text{fine}}, \underbrace{D_{\text{d}}(Z_v, Z_h)}_{\text{motion}} \right] \quad (4)$$

Here,  $\mathbf{f}_{t \rightarrow t+H}$  denotes the predicted object flow over a temporal horizon of  $H$ .  $Z_v$  denotes the extracted image feature maps from several historical frames  $o_{t-n \rightarrow t}$ , while  $H(\cdot)$  represents the heatmap computation module.  $S(\cdot)$  signifies the soft-sampling operation, which obtains the coarse flow

starting point  $\mathbf{f}_s$  by aggregating spatial coordinates weighted by the response values at each point of the heatmap. Based on this,  $Z_h$  is derived by computing local correlations between features across different temporal frames. Finally,  $D_{\text{off}}$  and  $D_{\text{d}}$  correspond to the two outputs of the flow decoder, representing the fine-grained refinement for the starting point and the flow displacement vector, respectively.

The predicted flow is then utilized to synthesize the future observation:

$$\hat{o}_{t+H} = \mathcal{F}(o_{t-n \rightarrow t}) = \text{Paint}(\mathbf{f}_{t \rightarrow t+H}, o_t) \quad (5)$$

where  $\mathcal{F}(\cdot)$  is the symbol of F2F module. The operation  $\text{Paint}(\cdot)$  represents the process of rendering the flow vectors  $\mathbf{f}_{t \rightarrow t+H}$  onto the current observation, where the vector is assigned a specific color to represent its magnitude and direction of displacement from its origin.

**Data Collection.** We utilize the UMI [6] device as the primary hardware for data collection, enabling rapid data acquisition for single-task policies. Furthermore, the fisheye images collected by UMI serve as the foundational training data for the flow predictor.

Regarding fisheye image processing, the SAM [28] image segmentation approach proved to be the most reliable model in our evaluations, compared to alternative methods such as point tracking [20], optical flow estimation [10], and filtering. We utilize a segmentation-and-clustering pipeline to extract the most representative keypoints of the interacting object as the starting points for ground truth flow, while the flow displacement is computed as the pixel-wise distance of these keypoints. Further details are provided in Appendix A.

In pick-and-place tasks, occlusion of objects by the grip-

per occurs frequently. However, existing segmentation and amodal [37] models fail to process occluded objects in fisheye images. To enable flow prediction under occlusion, we first obtain ground truth flow from gripper-free video sequences. Subsequently, we synthesize the training data by superimposing gripper masks onto these videos to generate the final observations, following [34].

### C. Flow Contrastive Learning

Although the predicted future observation  $\hat{\mathbf{o}}_{t+H}$  derived from Eq. 5 preserves comprehensive flow information, a naive concatenation of this prediction with the current observation may fail to yield a future-aware representation comparable to that of the real future observation  $\mathbf{o}_{t+H}$ . This representational discrepancy would confuse the policy and undermine our primary objective of synthesizing future observations for asynchronous inference.

To mitigate this, F2F incorporates a contrastive learning [27, 47] framework during the policy training phase, which aims to minimize the representation discrepancy between flow-painted future  $\hat{\mathbf{o}}_{t+H}$  and real future  $\mathbf{o}_{t+H}$ :

$$\min_{\theta} \text{Diff}(\mathcal{E}_{\theta}(\hat{\mathbf{o}}_{t+H}), \mathcal{E}_{\theta}(\mathbf{o}_{t+H})) \quad (6)$$

where  $\mathcal{E}$  is the encoder of policy. Diff indicates the difference in feature space. As illustrated in the contrastive learning module of Fig. 4, we compute the normalized cosine similarity between the latent features of the ground truth observations and the predicted observations. Specifically, both the predicted and ground truth observations share a common feature encoder but are mapped into the latent space via separate projectors. Our objective is to maximize the feature similarity for synchronized pairs while minimizing it for asynchronous pairs.

However, given the high visual correlation between adjacent frames, indiscriminately treating all temporally distinct features as negative samples is suboptimal. To address this, we design a temporal masking mechanism, denoted as  $\mathbf{M}$ , to filter out features from temporally proximal steps.

$$\mathbf{M}_{i,k} = \mathbb{I}(d(i,k) = 0 \vee d(i,k) \geq \tau) \quad (7)$$

where  $d(i,k)$  is the temporal distance between two frames and  $\tau$  is the distance threshold hyperparameter.

Consequently, the similarity is optimized exclusively for positive pairs and sufficiently distant true-negative pairs. Consequently, we define the directional contrastive loss  $\ell(u,v)$  with temporal mask  $\mathbf{M}$  as:

$$\ell(u,v) = -\frac{1}{N} \sum_{i=1}^N \log \frac{e^{\langle u_i, v_i \rangle / \tau}}{\sum_{k=1}^N \mathbf{M}_{i,k} \cdot e^{\langle u_i, v_k \rangle / \tau}} \quad (8)$$

Here, we define  $u = \mathcal{E}_{\theta}(o_i)$  and  $v = \mathcal{E}_{\theta}(\hat{o}_i)$  as the feature representations of the ground-truth observation and the predicted observation, respectively, extracted by the shared visual encoder  $\mathcal{E}_{\theta}$ . The term  $\langle u, v \rangle$  denotes the cosine similarity between these two embeddings.

The final symmetric objective is computed as the average of the bidirectional losses between predicted features  $z^p$  and

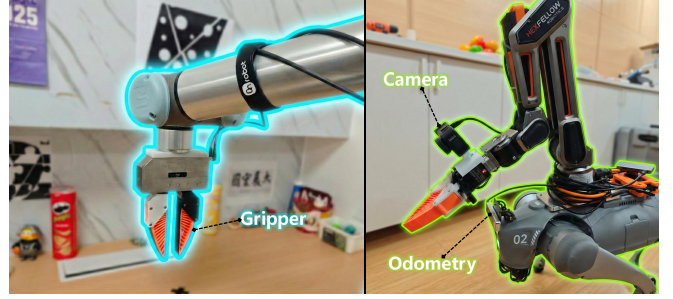


Fig. 5: **Hardware Platform.** F2F-AP is evaluated in fixed-base arm and quadruped manipulator equipped with camera and odometry.

ground truth features  $z^g$ :

$$\mathcal{L} = \frac{1}{2} [\ell(z^p, z^g) + \ell(z^g, z^p)] \quad (9)$$

### D. F2F Asynchronous Policy

**Policy Architecture.** The F2F policy is built upon the Diffusion Policy framework. It employs a pre-trained ViT as the encoder and a U-Net as the decoder to generate actions. The overall policy can be expressed by the following formulation:

$$\mathcal{P}(\hat{\mathbf{o}}_{t+H}, \mathbf{s}) = \mathcal{D} \circ \mathcal{E}(\mathcal{F}(\mathbf{o}_{t-n \rightarrow t}), \mathbf{s}) \quad (10)$$

where  $\mathcal{D}$  denotes the decoder within the policy. As depicted in Fig. 4, F2F-AP first synthesizes future observations via the flow predictor  $\mathcal{F}$ , followed by a Diffusion Policy to generate action trajectories.

Since the actions produced by F2F-AP are explicitly aligned with the real-world timeline, there is no need to discard the initial actions of each generation cycle. Instead, we directly maintain a queue of valid actions with real timestamps. Empowered by this future context, F2F generates trajectories that are oriented towards the future states of dynamic objects.

**Explicit Latency Modeling.** Since total latency of specific system is bounded normally, setting the latency parameter above this bound ensures predictions align with executable timelines beyond latency. F2F-AP calculates the required prediction horizon  $H$  based on the total latency  $\Delta_{\text{total}}$  and the control time step  $\delta_t$ :

$$H = \lceil \Delta_{\text{total}} / \delta_t \rceil \quad (11)$$

This derivation leads to the policy formulation presented in Eq. 4. In practice, all latency components can be estimated [6], which enables us to explicitly model the system latency.

## IV. EXPERIMENT

To assess the capability of F2F-AP in real-time dynamic scenarios, we designed five tasks for grasping moving objects, executed on two different robots. Through comparative experiments involving different inference modalities for imitation learning policies, we demonstrate that F2F-AP significantly enhances policy performance in real-time dynamic tasks.

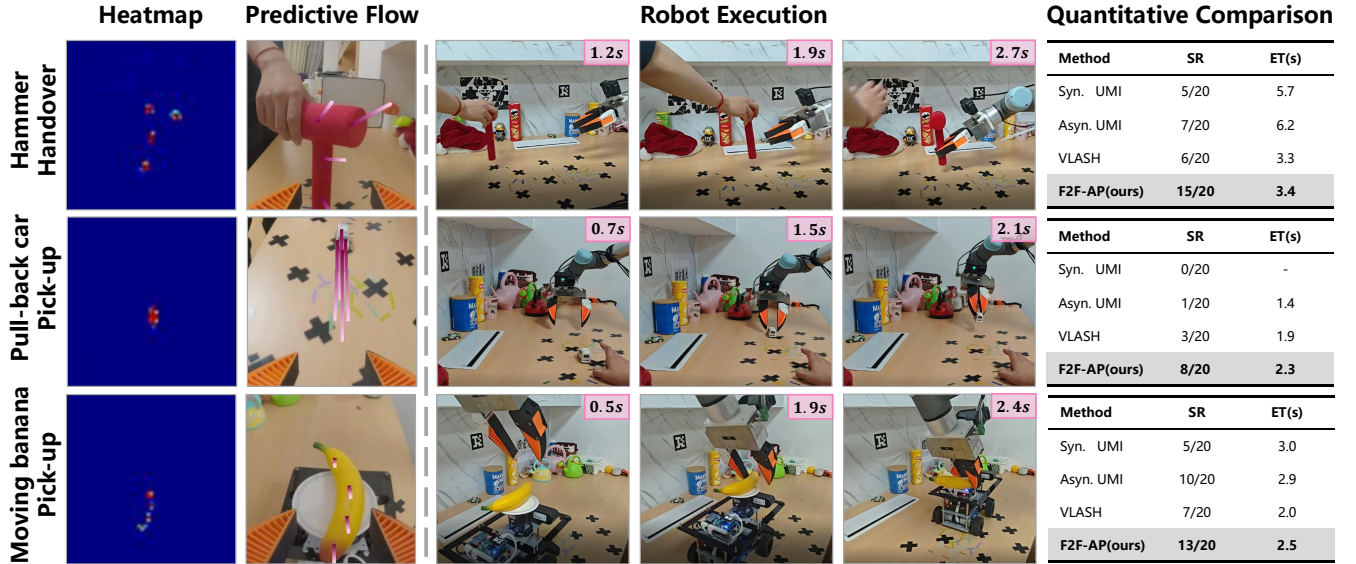


Fig. 6: **Visualization and quantitative results on the fixed-base robotic arm.** (Left) Visualization of heatmaps and predicted object flow during policy execution. In the  $56 \times 56$  resolution heatmaps, blue and red regions denote low and high responsiveness, respectively. The predicted flow is visualized using pink lines transitioning from dark to light. (Middle) Third-person perspective of the robot performing the task. The timestamp in the top-right corner indicates the elapsed time since the task started, highlighting the dynamic nature of the task and the robot’s responsiveness. (Right) Quantitative comparison results across different tasks, benchmarking F2F-AP and three baselines under identical experimental conditions.

### A. Experiment Settings

In this section, we detail the experimental baselines, evaluation metrics, and the platform setup used for validation.

**Platforms.** To demonstrate the versatility of our approach, we deploy it on two distinct robotic platforms, as illustrated in Fig. 5, encompassing both fixed-base tabletop and mobile manipulation scenarios.

- **Fixed-Base Robotic Arm.** Adhering to standard experimental configurations, we deploy the model on a static single-arm system. Specifically, we utilize the UR5e robotic arm for these experiments.
- **Quadruped Mobile Manipulator.** Addressing the challenges of mobile manipulation, we employ a Unitree Go2 quadruped robot integrated with an Hexfellow Saber robotic arm. This system is controlled by a robust Whole-Body Controller (WBC), which provides unified control over the joints of both the quadruped base and the arm to precisely track end-effector pose trajectories.

**Baseline methods.** We select UMI [6] for fixed-base robotic arm and UMI-on-Legs [15] for quadruped mobile manipulator as our baselines due to their consistent data collection method, and evaluate them under both synchronous and asynchronous inference settings. Additionally, we integrate the VLASH [35] method into the UMI policy, training it with future robot proprioception states. Finally, we construct F2F-AP by incorporating the F2F module and asynchronous inference architecture into UMI. For fair comparison, all models are trained on the same source dataset collected in a real-world environment.

**Metrics.** We employ two primary metrics to evaluate model

performance, specifically focusing on reliability and efficiency in dynamic scenarios.

- **Task Success Rate (SR).** To measure system reliability, SR is defined as the ratio of successfully completed trials to the total number of experimental attempts.
- **Average Execution Time (ET).** To evaluate efficiency, we calculate the average duration required to complete a task, measured from the onset of the first action to the successful termination of the episode. Note that this calculation exclusively includes successful trials.

### B. Evaluation in Fixed-Base Arm

Experiments conducted on the fixed-base robotic arm encompass three distinct aspects: human-to-robot handover, rapid response execution, and dynamic object tracking. The corresponding visualization and quantitative results are presented in Fig. 6.

The system exhibits an average latency profile of  $\Delta o \approx 125$  ms,  $\Delta i \approx 200$  ms, and  $\Delta c < 50$  ms in our experiment. Based on these measured delays and the action sampling interval  $\delta_t = 0.1s$ , we determine the future horizon parameter  $H = 4$  to ensure temporal alignment during asynchronous inference.

**Human-to-Robot Hammer Handover.** This task requires the robot to react swiftly to receive a hammer handed over by a human participant. In real-world scenarios, the handover process typically occurs in less than 1s, necessitating the robot to predict the interaction point based on the dynamic velocity of the moving object to minimize human waiting time. The experimenter intentionally averts their gaze from the robot gripper during testing. This protocol ensures task stochasticity

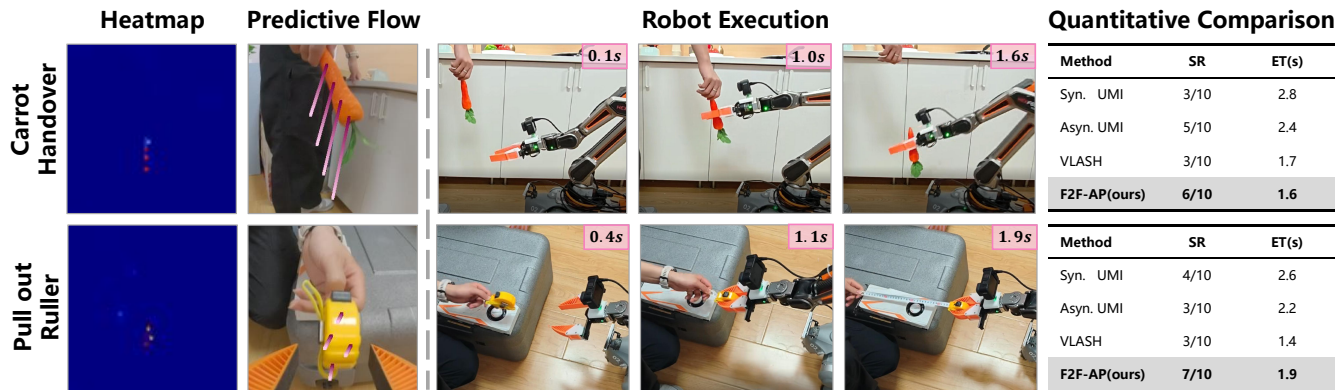


Fig. 7: **Visualization and quantitative results on the quadruped mobile manipulator.** Similar to Fig. 6, (Left) displays the heatmaps and predicted optical flow during policy execution. (Middle) shows the third-person perspective of the robot performing the task. (Right) presents the quantitative analysis and comparison across different tasks.

and eliminates potential human bias where participants might subconsciously compensate for the robot’s motion. The standard for a successful trial is that the hammer is clamped out and does not fall off.

Experimental results demonstrate that F2F-AP significantly outperforms the baseline methods in both success rate and average execution time, achieving superior smoothness and securing the hammer proactively.

**Pull-back Car Interception.** Intercepting a rapidly moving pull-back car presents a formidable challenge. The target toy-car features a restricted effective grasping region of merely  $5\text{cm}$  and travels at an average velocity of  $25\text{cm/s}$ . Consequently, the available interception window is constrained to under  $0.4\text{s}$ , which falls within the range of the inherent system latency. Furthermore, due to the stochastic nature of the vehicle’s velocity, the optimal grasping timing varies significantly across trials. This necessitates a policy capable of perceiving motion dynamics of the pull-back car to accurately anticipate the precise location and timing for gripper actuation. A trial is considered successful if the robot firmly grasps the vehicle and lifts it clear of the tabletop surface.

Results indicate that F2F-AP is highly competent in handling such highly dynamic and stochastic scenarios, effectively perceiving the car’s velocity to adaptively select the optimal timing for gripper actuation.

**Pick-up Moving Banana.** In this task, a banana is placed on a platform moving continuously forward, with the speed randomized across different episodes. To successfully grasp a target with such a constantly changing position, the policy must possess future perception capabilities. Otherwise, given the stochastic movement speeds, a policy relying solely on the current observations cannot accurately determine the interaction point or adjust the velocity of the robot to synchronize with the moving banana. A trial is considered successful if the robot firmly grasps the banana and lifts it without dropping.

Our evaluations show that F2F-AP achieves substantial improvements in success rate, demonstrating proactive motion capabilities and adapting effectively to the constantly varying speeds of the moving target.

**Analysis of Experiment Results.** Original UMI, when operating under a synchronous setting, exhibits slow responsiveness and struggles to complete time-sensitive tasks. Conversely, asynchronous UMI suffers from a dual misalignment of both proprioceptive states and RGB context. This leads to lagging and unsmooth trajectories, often characterized by repetitive attempts and jittery movements. While VLASH achieves smooth trajectory connections by incorporating future states, it still operates under an incorrect, delayed visual context. Consequently, it fails to generate actions that satisfy real-world temporal requirements, frequently manifesting as overshooting or missing the critical interaction timing altogether.

The varying success rates across these dynamic tasks is fundamentally caused by the impact of the training-inference gap caused by the system latency. During training, models are supervised using perfectly aligned actions and observations in the dataset. However, during inference, feeding lagging observations into the network naturally yields lagging actions. Furthermore, in highly dynamic tasks with limited training data, it is difficult for models to generalize across all possible motion variations. Once a model drifts into out-of-distribution states due to temporally mismatched actions, it inevitably produces cascading errors.

By fundamentally addressing this issue, F2F-AP explicitly aligns the visual observations and proprioceptive states to the moment of action execution. This alignment ensures that the inferred actions strictly meet the temporal requirements of the real world, guaranteeing the model’s robust adaptability to dynamic tasks even in the presence of inherent system latency.

### C. Evaluation in Quadruped Mobile Manipulator

We conducted two experiments on the quadruped mobile manipulator: a human-to-robot carrot handover and a collaborative task measuring the length of a graphics card. The corresponding visualizations and quantitative results are presented in Fig. 7.

Experimental measurements indicate that the latency profile of the quadruped mobile manipulator is comparable to that of

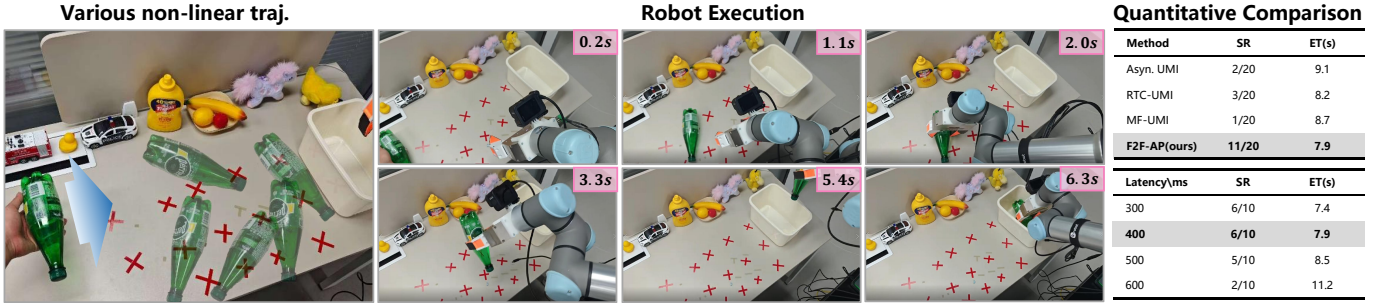


Fig. 8: **Visualization and quantitative results of the advanced experiment.** (Left) shows the diversity of trajectory. (Middle) shows a third-person view illustrating the entire process of grasping the bottle. (Right) is the quantitative results.

the fixed-base robotic arm system. Consequently, we retain the setting of  $H = 4$  as the future time horizon.

**Human-to-Robot Carrot handover.** Analogous to the task described in Sec. IV-B, this experiment requires the quadruped robot to react swiftly to receive a carrot handed over by a human, minimizing the human’s idle waiting time. We retain the blind-handover protocol, requiring participants to look away from the robot to preserve task stochasticity and prevent subconscious human adjustments from biasing the outcomes. The task is considered successful if the robot receives the carrot and maintains a secure grasp without dropping it.

Experimental results demonstrate that F2F-AP achieves measurable improvements in both success rate and response time compared to baseline methods, exhibiting proactive motion to the interaction point to complete the task. While UMI attains a comparable success rate under asynchronous inference, it incurs a longer execution time, and its performance degrades in the synchronous setting. Conversely, VLASH is prone to task failure due to over-shooting, which causes it to frequently miss the optimal interaction point. Further analysis of the quadruped experiments is provided in Sec. V.

**Collaborative Length Measurement.** The task requires the quadruped robot to sequentially execute three actions: grasping the tape measure, pressing it down firmly, and waiting for the human measurement. To ensure fluid collaboration, the robot must clamp the tape measure immediately upon handover and reposition itself to an optimal pose for measurement. The former phase demands rapid responsiveness to dynamic interactive objects, while the latter requires the policy to maintain stability without jitter as the human pulls the tape dynamically. Success is defined as the robot effectively clamping and repositioning the tape, maintaining a stable hold throughout the measurement process.

In F2F-AP, the Flow2Future module predicts object flow where the flow displacement closely correlates with the magnitude of the required action. Consequently, when the object remains stationary, F2F-AP infers from the zero-flow state that it should maintain a static pose, thereby exhibiting superior stability compared to other approaches. Experimental results confirm that F2F-AP achieves a significantly higher success rate than baseline methods which fail to maintain the necessary stability leads to their low success rates.

#### D. Advanced Dynamic Experiment

To further evaluate the model’s capabilities and elucidate the underlying reasons for its performance improvement, we conducted a more complex experiment on grasping a rolling, half-filled water bottle. Due to the randomness of human throws in height, force, and angle, alongside the bottle’s inherent asymmetry and complex internal fluid dynamics, the bottle exhibits a highly stochastic and non-linear trajectory, as illustrated in Fig. 8. Consequently, the model must explicitly anticipate the rolling bottle’s future position and execute precise proactive movements. A trial is considered successful if the robot securely grasps the rolling bottle and places it into the bin on the right.

Due to the incorrect observation context caused by system latency, the asynchronous UMI fails to generate appropriate actions for the dynamic object. While augmenting UMI with RTC [3] yields smoother motions, it cannot compensate for the delayed information, thus failing to significantly improve the experimental performance. Next, to rule out the possibility that F2F-AP’s gains stem merely from the additional visual frames introduced by the Flow2Future module, we evaluated a UMI variant called MF-UMI with its input frame count increased to match that of F2F-AP. This UMI variant yields even degraded performance, indicating that naively stacking historical frames is insufficient to improve model capability in the current setting.

In contrast, F2F-AP achieves overwhelmingly superior performance. This is because dynamic tasks are highly sensitive to latency, an issue that trajectory fusion methods like RTC cannot adequately address. Furthermore, simply attempting to fit the model to training data by incorporating more historical information is equally undesirable. On the one hand, it exacerbates the difficulty for the policy in modeling the mapping between observations and actions; on the other hand, directly utilizing historical frames introduces additional temporal uncertainty. As a result, the multi-frame UMI variant is almost entirely incapable of completing the rolling bottle task. F2F-AP, however, directly addresses the latency issue. By providing correctly timed observation context, it ensures that the inferred actions strictly meet the demanding requirements of a dynamically evolving environment. The findings strongly validate the effectiveness of our design, which explicitly lever-

TABLE I: **Ablation Studies.** The **upper section** reports results from the *Hammer Handover* task, while the **lower section** corresponds to the *Banana Picking* task in Sec. IV-B.

Method	SR	ET (s)
Low Freq. Inference	4/20	5.1
Low Contrastive Wt.	8/20	3.5
w/o Contrastive Loss	10/20	3.5
w/o heatmap.	6/20	3.1
<b>Full F2F-AP</b>	<b>15/20</b>	<b>3.4</b>
w/o Future State	5/20	3.3
MF-UMI	11/20	2.9
Diff. Line Color	13/20	2.5
Fewer Flow Points	11/20	2.4
<b>Full F2F-AP</b>	<b>13/20</b>	<b>2.5</b>

ages historical data to predict optical flow and construct future observations rather than simply consuming more frames.

Additionally, we tested F2F-AP under various latency conditions. The results demonstrate its robustness to different latency magnitudes; a significant drop in the success rate only occurs when the latency becomes excessively large and fundamentally incompatible with the dynamic task.

#### E. Ablation

To further validate the efficacy of our policy design, we conducted ablation studies targeting key components and hyperparameters, with results summarized in Table I.

**Experimental Setup.** We first evaluated three main modules: asynchronous inference, flow predictor and contrastive learning mechanisms on the *Hammer Handover* task. Subsequently, we investigated hyperparameters such as flow line color and the number of flow points using the *Banana Picking* task. Additionally, we test the function of future state, and evaluate the performance of the original UMI when naively increasing its input frame count to match that of F2F-AP.

**Result Analysis.** In the ablation study of key modules, we observe that lowering the inference frequency undermines the benefits of the asynchronous architecture, thereby hindering the system’s ability to handle highly dynamic tasks. Furthermore, omitting contrastive learning or reducing its loss weight impedes the effective feature-level alignment between flow-based predicted observations and ground-truth observations, which directly leads to a drop in success rate. And removing the multi-branch heatmap architecture from the flow predictor prevents the model from converging to reasonable predictions, resulting in significant performance degradation.

Regarding hyperparameter sensitivity, we modified the flow color from pink to green and reduced the number of flow points from four to two. Experimental results demonstrate that variations in flow line color and the number of flow points have a negligible impact on performance, underscoring the robustness of the F2F-AP design. However, excluding the future proprioception state creates a misalignment between visual observations and the robot’s physical status, which degrades the success rate. And we additionally evaluated the MF-UMI. The performance gain of F2F-AP over MF-UMI

here is not as substantial as that in Sec. IV-D. This stems from the near-linear simplicity of the task, where even the naive UMI performs similarly well. Nevertheless, F2F-AP still achieves an absolute improvement of 10%.

#### V. LIMITATION AND FUTURE WORKS

While F2F-AP empowers the policy to infer future actions directly from predicted observations, several challenges remain for robust real-world deployment.

First, F2F-AP explicitly models the total system latency,  $\Delta_{total}$ , to determine the prediction horizon  $H$ . In practice, while fixed-base robotic arms exhibit stable latency, complex platforms like quadruped mobile manipulators suffer from significant latency uncertainty. Such stochastic latency can undermine the effectiveness of our fixed-horizon approach. Future work aims to develop an active latency perception mechanism that dynamically adjusts the prediction horizon  $H$  based on real-time delay measurements, thereby allowing F2F-AP to evolve into a prediction model that accepts the future time step as an explicit input.

Second, F2F-AP is currently limited to single-task scenarios, requiring a specifically trained flow predictor for each distinct task. This constraint hinders the scalability of our method toward more powerful, generalist models. To address this, future works could design a universal object flow predictor capable of generating task-conditioned flow, enabling the synthesis of future observations across diverse tasks.

Finally, F2F-AP operates as a 2D vision-based method, with object flow estimation confined to the 2D pixel space. Future work will extend F2F-AP framework to support 3D inputs. By predicting object flow within 3D space, we aim to lift representations from the pixel space into real-world coordinates, endowing the model with superior spatial understanding.

#### VI. CONCLUSION

In this work, we introduced the Flow-to-Future Asynchronous Policy (F2F-AP). Within an asynchronous inference framework, F2F-AP incorporates the Flow2Future module, which utilizes object flow estimation to directly synthesize future observations, thereby enabling the generation of future-aware action chunks. To ensure robustness, we developed a heatmap-based model to stabilize flow prediction and employed flow contrastive learning to minimize the feature discrepancy between predicted and ground-truth observations. Through extensive experiments across two distinct robotic platforms, our results demonstrate that F2F-AP significantly enhances success rates in dynamic tasks while reducing task execution time and improving system responsiveness. These findings highlight object flow as a powerful tool for bridging the gap between the current and the future. By acquiring future observations, the model is endowed with enhanced capabilities to handle dynamic environments.

#### REFERENCES

- [1] Shikhar Bahl, Russell Mendonca, Lili Chen, Unnat Jain, and Deepak Pathak. *Affordances from Human Videos*

- as a Versatile Representation for Robotics. In *2023 IEEE/CVF Conference on Computer Vision and Pattern Recognition (CVPR)*, pages 01–13, Vancouver, BC, Canada, June 2023. IEEE. ISBN 979-8-3503-0129-8.
- [2] Homanga Bharadhwaj, Roozbeh Mottaghi, Abhinav Gupta, and Shubham Tulsiani. Track2act: Predicting point tracks from internet videos enables generalizable robot manipulation. In Aleš Leonardis, Elisa Ricci, Stefan Roth, Olga Russakovsky, Torsten Sattler, and Gül Varol, editors, *Computer Vision – ECCV 2024*, pages 306–324, Cham, 2025. Springer Nature Switzerland. ISBN 978-3-031-73116-7.
- [3] Kevin Black, Manuel Y Galliker, and Sergey Levine. Real-time execution of action chunking flow policies.
- [4] Kevin Black, Allen Z. Ren, Michael Equi, and Sergey Levine. **Training-Time Action Conditioning for Efficient Real-Time Chunking**, December 2025.
- [5] Cheng Chi, Zhenjia Xu, Siyuan Feng, Eric Cousineau, Yilun Du, Benjamin Burchfiel, Russ Tedrake, and Shuran Song. **Diffusion Policy: Visuomotor Policy Learning via Action Diffusion**, March 2024.
- [6] Cheng Chi, Zhenjia Xu, Chuer Pan, Eric Cousineau, Benjamin Burchfiel, Siyuan Feng, Russ Tedrake, and Shuran Song. **Universal Manipulation Interface: In-The-Wild Robot Teaching Without In-The-Wild Robots**. *CoRR*, January 2024.
- [7] Ethan Chun, Yilun Du, Anthony Simeonov, Tomas Lozano-Perez, and Leslie Kaelbling. **Local Neural Descriptor Fields: Locally Conditioned Object Representations for Manipulation**. In *2023 IEEE International Conference on Robotics and Automation (ICRA)*, pages 1830–1836, May 2023.
- [8] Karthik Dharmarajan, Wenlong Huang, Jiajun Wu, Li Fei-Fei, and Ruohan Zhang. **Dream2Flow: Bridging Video Generation and Open-World Manipulation with 3D Object Flow**, December 2025.
- [9] Thanh-Toan Do, Anh Nguyen, and Ian Reid. **AffordanceNet: An End-to-End Deep Learning Approach for Object Affordance Detection**. In *2018 IEEE International Conference on Robotics and Automation (ICRA)*, pages 5882–5889, May 2018.
- [10] Qiaole Dong and Yanwei Fu. **MemFlow: Optical Flow Estimation and Prediction with Memory**, April 2024.
- [11] Ben Eisner, Harry Zhang, and David Held. **FlowBot3D: Learning 3D Articulation Flow to Manipulate Articulated Objects**, May 2024.
- [12] Kuan Fang, Fangchen Liu, Pieter Abbeel, and Sergey Levine. **MOKA: Open-World Robotic Manipulation through Mark-Based Visual Prompting**. In *Robotics: Science and Systems XX*. Robotics: Science and Systems Foundation, July 2024. ISBN 979-8-9902848-0-7.
- [13] Wei Gao and Russ Tedrake. **kPAM 2.0: Feedback Control for Category-Level Robotic Manipulation**. *IEEE Robotics and Automation Letters*, 6(2):2962–2969, April 2021. ISSN 2377-3766.
- [14] Tuba Girgin and Emre Uğur. **Multiobject Graph Affordance Network: Goal-Oriented Planning Through Learned Compound Object Affordances**. *IEEE Transactions on Cognitive and Developmental Systems*, 17(4): 847–858, August 2025. ISSN 2379-8939.
- [15] Huy Ha, Yihuai Gao, Zipeng Fu, Jie Tan, and Shuran Song. **UMI on Legs: Making Manipulation Policies Mobile with Manipulation-Centric Whole-body Controllers**. In *CoRL 2024 Workshop on Whole-Body Control and Bimanual Manipulation: Applications in Humanoids and Beyond*, November 2024.
- [16] Wenlong Huang, Chen Wang, Ruohan Zhang, Yunzhu Li, Jiajun Wu, and Li Fei-Fei. **Voxposer: Composable 3d value maps for robotic manipulation with language models**.
- [17] Wenlong Huang, Yu-Wei Chao, Arsalan Mousavian, Ming-Yu Liu, Dieter Fox, Kaichun Mo, and Li Fei-Fei. **PointWorld: Scaling 3D World Models for In-The-Wild Robotic Manipulation**, January 2026.
- [18] Physical Intelligence, Kevin Black, Noah Brown, James Darpinian, Karan Dhabalia, Danny Driess, Adnan Esmail, Michael Equi, Chelsea Finn, Niccolo Fusai, Manuel Y. Galliker, Dibya Ghosh, Lachy Groom, Karol Hausman, Brian Ichter, Szymon Jakubczak, Tim Jones, Liyiming Ke, Devin LeBlanc, Sergey Levine, Adrian Li-Bell, Mohith Mothukuri, Suraj Nair, Karl Pertsch, Allen Z. Ren, Lucy Xiaoyang Shi, Laura Smith, Jost Tobias Springenberg, Kyle Stachowicz, James Tanner, Quan Vuong, Homer Walke, Anna Walling, Haohuan Wang, Lili Yu, and Ury Zhilinsky.  **$\pi_{0.5}$ : a Vision-Language-Action Model with Open-World Generalization**, April 2025.
- [19] Yuanchen Ju, Kaizhe Hu, Guowei Zhang, Gu Zhang, Mingrun Jiang, and Huazhe Xu. **Robo-ABC: Affordance Generalization Beyond Categories via Semantic Correspondence for Robot Manipulation**, January 2024.
- [20] Nikita Karaev, Iurii Makarov, Jianyuan Wang, Natalia Neverova, Andrea Vedaldi, and Christian Rupprecht. **CoTracker3: Simpler and Better Point Tracking by Pseudo-Labeling Real Videos**, October 2024.
- [21] Weijie Kong, Qi Tian, Zijian Zhang, Rox Min, Zuozhuo Dai, Jin Zhou, Jiangfeng Xiong, Xin Li, Bo Wu, Jianwei Zhang, Kathrina Wu, Qin Lin, Junkun Yuan, Yanxin Long, Aladdin Wang, Andong Wang, Changlin Li, Duo-jun Huang, Fang Yang, Hao Tan, Hongmei Wang, Jacob Song, Jiawang Bai, Jianbing Wu, Jinbao Xue, Joey Wang, Kai Wang, Mengyang Liu, Pengyu Li, Shuai Li, Weiyan Wang, Wenqing Yu, Xincheng Deng, Yang Li, Yi Chen, Yutao Cui, Yuanbo Peng, Zhentao Yu, Zhiyu He, Zhiyong Xu, Zixiang Zhou, Zunnan Xu, Yangyu Tao, Qinglin Lu, Songtao Liu, Dax Zhou, Hongfa Wang, Yong Yang, Di Wang, Yuhong Liu, Jie Jiang, and Caesar Zhong. **HunyuanVideo: A Systematic Framework For Large Video Generative Models**, March 2025.
- [22] Aileen Liao, Dong-Ki Kim, Max Olan Smith, Ali-akbar Agha-mohammadi, and Shayegan Omidshafiei. **Delay-Aware Diffusion Policy: Bridging the Observation-**

- Execution Gap in Dynamic Tasks, December 2025.
- [23] Kaichun Mo, Leonidas J. Guibas, Mustafa Mukadam, Abhinav Gupta, and Shubham Tulsiani. **Where2Act: From Pixels to Actions for Articulated 3D Objects**. In *Proceedings of the IEEE/CVF International Conference on Computer Vision*, pages 6813–6823, 2021.
- [24] Soroush Nasiriany, Sean Kirmani, Tianli Ding, Laura Smith, Yuke Zhu, Danny Driess, Dorsa Sadigh, and Ted Xiao. **RT-Affordance: Affordances are Versatile Intermediate Representations for Robot Manipulation**, November 2024.
- [25] Chuer Pan, Brian Okorn, Harry Zhang, Ben Eisner, and David Held. **TAX-Pose: Task-Specific Cross-Pose Estimation for Robot Manipulation**. In *Proceedings of The 6th Conference on Robot Learning*, pages 1783–1792. PMLR, March 2023.
- [26] Shengyi Qian, Weifeng Chen, Min Bai, Xiong Zhou, Zhuowen Tu, and Li Erran Li. **AffordanceLLM: Grounding Affordance from Vision Language Models**. In *2024 IEEE/CVF Conference on Computer Vision and Pattern Recognition Workshops (CVPRW)*, pages 7587–7597, Seattle, WA, USA, June 2024. IEEE. ISBN 979-8-3503-6547-4.
- [27] Alec Radford, Jong Wook Kim, Chris Hallacy, Aditya Ramesh, Gabriel Goh, Sandhini Agarwal, Girish Sastry, Amanda Askell, Pamela Mishkin, Jack Clark, Gretchen Krueger, and Ilya Sutskever. **Learning Transferable Visual Models From Natural Language Supervision**. In *Proceedings of the 38th International Conference on Machine Learning*, pages 8748–8763. PMLR, July 2021.
- [28] Nikhila Ravi, Valentin Gabeur, Yuan-Ting Hu, Ronghang Hu, Chaitanya Ryali, Tengyu Ma, Haitham Khedr, Roman Rädle, Chloe Rolland, Laura Gustafson, Eric Mintun, Junting Pan, Kalyan Vasudev Alwala, Nicolas Carion, Chao-Yuan Wu, Ross Girshick, Piotr Dollár, and Christoph Feichtenhofer. **SAM 2: Segment Anything in Images and Videos**, October 2024.
- [29] Kohei Sendai, Maxime Alvarez, Tatsuya Matsushima, Yutaka Matsuo, and Yusuke Iwasawa. **Leave No Observation Behind: Real-time Correction for VLA Action Chunks**, September 2025.
- [30] Mustafa Shukor, Dana Aubakirova, Francesco Capuano, Pepijn Kooijmans, Steven Palma, Adil Zouitine, Michel Aractingi, Caroline Pascal, Martino Russi, Andres Marafioti, Simon Alibert, Matthieu Cord, Thomas Wolf, and Remi Cadene. **SmolVLA: A Vision-Language-Action Model for Affordable and Efficient Robotics**, June 2025.
- [31] Anthony Simeonov, Yilun Du, Andrea Tagliasacchi, Joshua B. Tenenbaum, Alberto Rodriguez, Pulkit Agrawal, and Vincent Sitzmann. **Neural Descriptor Fields: SE(3)-Equivariant Object Representations for Manipulation**, December 2021.
- [32] Anukriti Singh, Kasra Torshizi, Khuzema Habib, Kelin Yu, Ruohan Gao, and Pratap Tokekar. **AFFORD2ACT: Affordance-Guided Automatic Keypoint Selection for Generalizable and Lightweight Robotic Manipulation**, October 2025.
- [33] Yue Su, Xinyu Zhan, Hongjie Fang, Yong-Lu Li, Cewu Lu, and Lixin Yang. **Motion Before Action: Diffusing Object Motion as Manipulation Condition**, April 2025.
- [34] Wei-En Tai, Yu-Lin Shih, Cheng Sun, Yu-Chiang Frank Wang, and Hwann-Tzong Chen. **Segment Anything, Even Occluded**, March 2025.
- [35] Jiaming Tang, Yufei Sun, Yilong Zhao, Shang Yang, Yujun Lin, Zhuoyang Zhang, James Hou, Yao Lu, Zhijian Liu, and Song Han. **VLASH: Real-Time VLAs via Future-State-Aware Asynchronous Inference**, November 2025.
- [36] Weiliang Tang, Jia-Hui Pan, Wei Zhan, Jianshu Zhou, Huaxiu Yao, Yun-Hui Liu, Masayoshi Tomizuka, Mingyu Ding, and Chi-Wing Fu. **Embodiment-agnostic Action Planning via Object-Part Scene Flow**. In *2025 IEEE International Conference on Robotics and Automation (ICRA)*, pages 2086–2093, May 2025.
- [37] Minh Tran. Aisformer: Amodal instance segmentation with transformer.
- [38] Team Wan, Ang Wang, Baole Ai, Bin Wen, Chaojie Mao, Chen-Wei Xie, Di Chen, Feiwu Yu, Haiming Zhao, Jianxiao Yang, Jianyuan Zeng, Jiayu Wang, Jingfeng Zhang, Jingren Zhou, Jinkai Wang, Jixuan Chen, Kai Zhu, Kang Zhao, Keyu Yan, Lianghua Huang, Mengyang Feng, Ningyi Zhang, Pandeng Li, Pingyu Wu, Ruihang Chu, Ruili Feng, Shiwei Zhang, Siyang Sun, Tao Fang, Tianxing Wang, Tianyi Gui, Tingyu Weng, Tong Shen, Wei Lin, Wei Wang, Wei Wang, Wenmeng Zhou, Wenting Wang, Wenting Shen, Wenyuan Yu, Xianzhong Shi, Xiaoming Huang, Xin Xu, Yan Kou, Yangyu Lv, Yifei Li, Yijing Liu, Yiming Wang, Yingya Zhang, Yitong Huang, Yong Li, You Wu, Yu Liu, Yulin Pan, Yun Zheng, Yuntao Hong, Yupeng Shi, Yutong Feng, Zeyinzi Jiang, Zhen Han, Zhi-Fan Wu, and Ziyu Liu. **Wan: Open and Advanced Large-Scale Video Generative Models**, April 2025.
- [39] Haoxuan Wang, Gengyu Zhang, Yan Yan, Yuzhang Shang, Ramana Rao Kompella, and Gaowen Liu. **Real-Time Robot Execution with Masked Action Chunking**, January 2026.
- [40] Chuan Wen, Xingyu Lin, John So, Kai Chen, Qi Dou, Yang Gao, and Pieter Abbeel. **Any-point Trajectory Modeling for Policy Learning**, July 2024.
- [41] Thomas Weng, David Held, Franziska Meier, and Mustafa Mukadam. **Neural Grasp Distance Fields for Robot Manipulation**. In *2023 IEEE International Conference on Robotics and Automation (ICRA)*, pages 1814–1821, May 2023.
- [42] Zhenyu Wu, Yuheng Zhou, Xiuwei Xu, Ziwei Wang, and Haibin Yan. **MoManipVLA: Transferring Vision-language-action Models for General Mobile Manipulation**. In *Proceedings of the Computer Vision and Pattern Recognition Conference*, pages 1714–1723, 2025.
- [43] Haozhe Xie, Beichen Wen, Jiarui Zheng, Zhaoxi Chen,

- Fangzhou Hong, Haiwen Diao, and Ziwei Liu. **DynamicVLA: A Vision-Language-Action Model for Dynamic Object Manipulation**, January 2026.
- [44] Mengda Xu, Zhenjia Xu, Yinghao Xu, Cheng Chi, Gordon Wetzstein, Manuela Veloso, and Shuran Song. **Flow as the Cross-Domain Manipulation Interface**, October 2024.
- [45] Zhuoyi Yang, Jiayan Teng, Wendi Zheng, Ming Ding, Shiyu Huang, Jiazheng Xu, Yuanming Yang, Wenyi Hong, Xiaohan Zhang, Guanyu Feng, Da Yin, Yuxuan Zhang, Weihang Wang, Yean Cheng, Bin Xu, Xiaotao Gu, Yuxiao Dong, and Jie Tang. **CogVideoX: Text-to-Video Diffusion Models with An Expert Transformer**, March 2025.
- [46] Chengbo Yuan, Chuan Wen, Tong Zhang, and Yang Gao. **General Flow as Foundation Affordance for Scalable Robot Learning**. In *8th Annual Conference on Robot Learning*, September 2024.
- [47] Chubin Zhang, Jianan Wang, Zifeng Gao, Yue Su, Tianru Dai, Cai Zhou, Jiwen Lu, and Yansong Tang. **CLAP: Contrastive Latent Action Pretraining for Learning Vision-Language-Action Models from Human Videos**, January 2026.
- [48] Fan Zhang and Michael Gienger. **Affordance-based Robot Manipulation with Flow Matching**, November 2025.
- [49] Junjie Zhang, Chenjia Bai, Haoran He, Zhigang Wang, Bin Zhao, Xiu Li, and Xuelong Li. **SAM-E: Leveraging Visual Foundation Model with Sequence Imitation for Embodied Manipulation**. In *Proceedings of the 41st International Conference on Machine Learning*, pages 58579–58598. PMLR, July 2024.
- [50] Tony Z. Zhao, Vikash Kumar, Sergey Levine, and Chelsea Finn. **Learning Fine-Grained Bimanual Manipulation with Low-Cost Hardware**. In *ICML Workshop on New Frontiers in Learning, Control, and Dynamical Systems*, July 2023.
- [51] Hongyan Zhi, Peihao Chen, Siyuan Zhou, Yubo Dong, Quanxi Wu, Lei Han, and Mingkui Tan. **3DFlowAction: Learning Cross-Embodiment Manipulation from 3D Flow World Model**, June 2025.

### A. Data Details

Data collection was performed manually using a UMI interface equipped with a GoPro fisheye camera and a gripper. For each task, we collected 100  $\sim$  200 trajectories to train both the F2F module and the policy, resulting in a total video duration of only about 10 minutes. Additionally, to obtain flow ground truth under occlusion, we captured a separate dataset using the fisheye camera without gripper, which is equivalent in size to the UMI dataset. This dataset is then utilized to generate synthetic training samples by overlaying gripper masks onto the images.

The procedure for acquiring flow ground truth is outlined in the pseudocode 1.

---

#### Algorithm 1 Ground Truth Flow Generation Pipeline

---

**Require:** RGB Video Sequence  $\mathcal{V} = \{I_1, \dots, I_T\}$ , Prediction Horizon  $H$

**Ensure:** Flow Ground Truth  $\mathcal{G}_{flow}$

- 1: **Initialization:** Human annotates bounding box  $\mathbf{b}_1$  on  $I_1$
  - 2:  $\triangleright$  Obtain object masks via SAM tracking
  - 3:  $\mathcal{M}_{1:T} \leftarrow \text{SAM-Track}(\mathcal{V}, \mathbf{b}_1)$
  - 4: Initialize keypoints set  $\mathcal{P}_0 \leftarrow \emptyset$
  - 5:  $\triangleright$  Extract temporal-consistent keypoints
  - 6: **for**  $t = 1$  to  $T$  **do**
  - 7:   **if**  $t = 1$  **then**
  - 8:     Init centroids  $\mathbf{c}_{init}$  randomly within  $\mathcal{M}_1$
  - 9:   **else**
  - 10:     Init centroids  $\mathbf{c}_{init} \leftarrow \mathcal{P}_{t-1}$   $\triangleright$  Use previous points as initialization
  - 11:      $\mathcal{P}_t \leftarrow \text{K-Means}(\mathcal{M}_t, K = 4, \text{init} = \mathbf{c}_{init})$
  - 12:      $\triangleright$  Compute flow labels
  - 13:  $\mathcal{G}_{flow} \leftarrow \emptyset$
  - 14: **for**  $t = 1$  to  $T - H$  **do**
  - 15:    $\mathcal{P}_{future} \leftarrow \mathcal{P}_{t+H}$
  - 16:    $\Delta\mathcal{P}_t \leftarrow \mathcal{P}_{future} - \mathcal{P}_t$   $\triangleright$  Calculate displacement
  - 17:    $GT_t \leftarrow \{(\mathbf{p}, \mathbf{d}) \mid \mathbf{p} \in \mathcal{P}_t, \mathbf{d} \in \Delta\mathcal{P}_t\}$
  - 18:    $\mathcal{G}_{flow} \leftarrow \mathcal{G}_{flow} \cup GT_t$
  - 19: **return**  $\mathcal{G}_{flow}$
- 

The data collected by UMI can be utilized for training both the policy and the flow predictor. To address severe occlusions caused by the gripper—for example, when the teapot held by the gripper completely obscures the cup during a pouring task—we supplement the dataset with gripper-free videos recorded via a fisheye camera. In practice, training the F2F module requires only about 10 minutes to achieve strong performance, as such data can be easily collected or sourced directly from the Internet.

Inspired by SAMEO, the specific procedure for obtaining the RGB ground truth from the pure fisheye videos is as follows. We randomly select and overlay pre-segmented gripper instances onto the videos to generate data identical to the original UMI captures. This process is illustrated in Fig. 9.

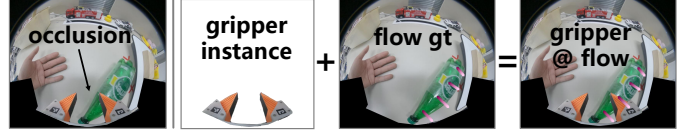


Fig. 9: Select a pre-segmented gripper instance and overlay it onto the original fisheye videos to generate the RGB ground truth

### B. Model Architecture

**Flow2Future Module.** The Flow2Future(F2F) module operates on an input video sequence  $V \in \mathbb{R}^{6 \times 224 \times 224 \times 3}$ . Initially, each frame is partitioned into  $16 \times 16$  non-overlapping patches and linearly projected to an embedding dimension of  $D = 384$ , augmented with learnable 2D spatial and 1D temporal sinusoidal positional embeddings. These tokenized representations are then processed by the backbone, which is an 8-layer BERT-style Transformer encoder. Specifically, the encoder is configured with 8 attention heads, a hidden dimension of 384, and an MLP intermediate dimension of 1536, utilizing a Pre-Norm structure with GELU activation.

For flow estimation, the HeatmapFlowDecoder first computes a local correlation volume within a search radius of  $r = 2$  between the current and all of the past frame features. Subsequently, this volume is processed by a heatmap prediction branch—comprising a standard convolutional block followed by transposed convolution layers—to output a probability heatmap. Upon extracting the keypoints via weighted K-Means, the corresponding features are sampled and fed into the flow regression MLP, which outputs the final sub-pixel offsets and flow vectors.

**Policy.** Our policy architecture adopts the UMI framework[6], utilizing a CLIP-pretrained ViT-Base encoder for observation encoding and a 1D Conditional U-Net for action generation. The policy operates on flow-augmented RGB images. Specifically, for each timestep in the observation horizon ( $T_{obs} = 2$ ), the frozen Flow2Future module predicts flow based on a history of  $T_{pred} = 6$  frames and overlays the resulting flow vectors onto the visual input. We employ a DDIM scheduler with 16 inference steps for diffusion generation process.

### C. Implementation Details.

**Training.** Firstly, The Flow2Future Module is trained using the Adam optimizer with a batch size of 32 and a base learning rate of  $1 \times 10^{-4}$ . We utilize a cosine annealing schedule with a 5-epoch warmup and enable mixed-precision training. The training objective combines an auxiliary image reconstruction loss, which encourages the model to capture global spatial context by restoring masked patches.

Then the policy is trained using the AdamW optimizer with a batch size of 32. We employ a cosine schedule with a 2000-step warmup, setting the base learning rate to  $3 \times 10^{-4}$  while applying a reduced rate of  $3 \times 10^{-5}$  to the vision backbone. The training objective incorporates a standard denoising loss and

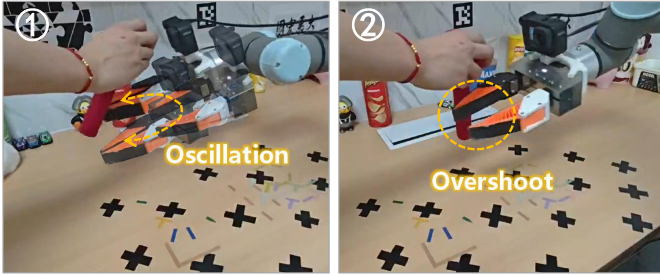


Fig. 10: **Comparative Visualization** of baseline failure modes: (1) Naive Asynchronous Inference, and (2) VLASH.



Fig. 11: **Extended Task.** Grasping a chip can rolling down a ramp. The objective is to grasp the moving can and subsequently return to the starting pose.

an auxiliary flow-contrastive loss—a key innovation of F2F-AP designed to align the embedding of the current observation with that of the future observation.

**Inference.** We execute our model on an NVIDIA RTX 3090 GPU with an inference frequency of 5 Hz, a standard rate for vision-based robotic manipulation. Meanwhile, the Whole-Body Controller of the quadruped mobile manipulator operates on an onboard NVIDIA Jetson Orin edge device.

#### D. Extended Evaluation.

**Comparative Analysis.** We documented the failure modes of Naive Asynchronous Inference and VLASH to provide a comparison with F2F-AP. Notably, all three methods were evaluated at the same inference frequency. As illustrated in Fig. 10, Naive Asynchronous Inference fails to generate temporally coherent actions due to system latency, manifesting as persistent grasping attempts that consistently miss the precise target location. In contrast, VLASH, lacking future observations, fails to anticipate the optimal stopping position in time, frequently resulting in overshooting.

**More Experiments.** We conducted an additional qualitative experiment involving grasping a rolling chip can to further validate the adaptability of F2F-AP to diverse object dynamics. The results demonstrate that F2F-AP exhibits superior performance and robust adaptability in this extended scenario, as shown in Fig. 11.

#### E. Failure Case Analysis

We categorize the four typical failure modes encountered during the deployment of F2F-AP, as illustrated in Fig. 12:

- 1) **Object Slippage.** Suboptimal grasping poses often result in insecure contact, causing the object to be ejected or slip out of the gripper during the closing phase.

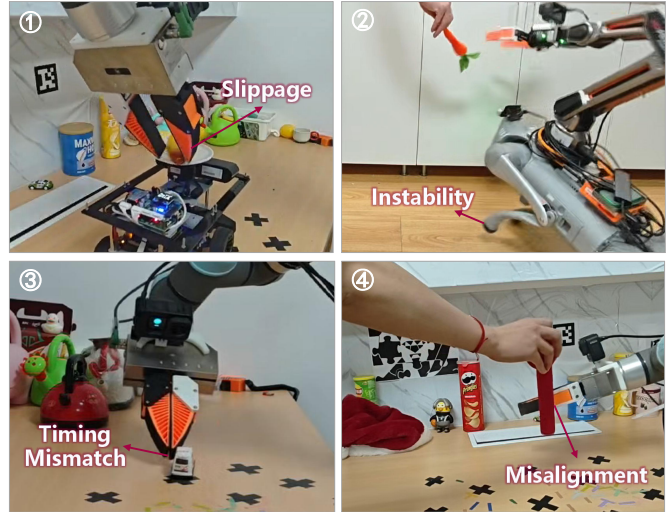


Fig. 12: **Failure Case Visualization** illustrates four representative failure scenarios in different tasks.

- 2) **System Instability.** Interacting with dynamic objects introduces significant kinetic disturbances. When coupled with the inherent instability of the hardware, especially for the Whole-Body Controller of the quadruped manipulator, rapid posture adjustments can lead to the loss of balance or system tipping.
- 3) **Timing Mismatch.** For dynamic tasks constrained by narrow interaction windows, errors in gripper actuation constitute the primary cause of task failure.
- 4) **Spatial Misalignment.** The policy may occasionally fail to achieve precise spatial alignment with the target interaction point, resulting in the end-effector missing the object entirely.